Published OnlineFirst June 18, 2015; DOI: 10.1158/0008-5472.CAN-15-0248

Integrated Systems and Technologies

Cancer Research

An Autoimmune Response Signature Associated with the Development of Triple-Negative Breast Cancer Reflects Disease Pathogenesis

Hiroyuki Katayama[1], Clayton Boldt[1], Jon J. Ladd[2], Melissa M. Johnson[3], Timothy Chao[2], Michela Capello[1], Jinfeng Suo[1], Jianning Mao[3], JoAnn E. Manson[4], Ross Prentice[2], Francisco Esteva[5], Hong Wang[1], Mary L. Disis[3], and Samir Hanash[1]

Abstract

The repertoire of antigens associated with the development of an autoimmune response in breast cancer has relevance to detection and treatment strategies. We have investigated the occurrence of autoantibodies associated with the development of triple-negative breast cancer (TNBC) in the before diagnosis setting and in samples collected at the time of diagnosis of TNBC. Lysate arrays containing protein fractions from the TNBC MDA-MB-231 cell line were hybridized with TNBC plasmas from the Women's Health Initiative cohort, collected before clinical diagnosis and with plasmas from matched controls. An immune response directed against spliceosome and glycolysis proteins was observed with case plasmas as previously reported in estrogen receptor$^+$ breast cancer. Importantly, autoantibodies directed against networks involving BRCA1, TP53, and cytokeratin proteins associated with a mesenchymal/basal phenotype were distinct to TNBC before diagnosis samples. Concordant autoantibody findings were observed with mouse plasma samples collected before occurrence of palpable tumors from a C3(1)-T triple negative mouse model. Plasma samples collected at the time of diagnosis of stage II TNBC and from matched healthy controls were subjected to proteomic analysis by mass spectrometry to identify Ig-bound proteins yielding a predominance of cytokeratins, including several associated with a mesenchymal/basal phenotype among cases compared with controls. Our data provide evidence indicative of a dynamic repertoire of antigens associated with a humoral immune response reflecting disease pathogenesis in TNBC. *Cancer Res; 75(16); 3246–54. ©2015 AACR.*

Introduction

The use of samples collected in before diagnosis setting, obtained before onset of symptoms, from prospective cohorts has the potential to identify biomarkers that are particularly relevant for early cancer detection (1). Moreover, refined genetically engineered mouse (GEM) models of human cancer that recapitulate their human counterparts offer a potential discovery and filtering engine for prioritization of candidate markers discovered in parallel using human specimens (2). A promising source of circulating cancer biomarkers stems from harnessing the humoral immune response directed against tumor antigens for the development of marker panels that have use for early cancer detection (3–6). The biologic significance of the humoral immune response in promoting or suppressing tumor development remains unclear (7, 8). Nevertheless, the discovery of potential antigens associated with an autoimmune response has led in some cases to successful validation studies aimed at assessing their potential diagnostic use (6, 9).

The full repertoire of antigens and epitopes associated with the development of autoantibodies and their specificity to particular cancer types remain largely undetermined (10, 11). We previously assessed the autoantibody repertoire exhibited in before diagnosis samples from subjects that subsequently developed estrogen receptor (ER)$^+$ progesterone receptor (PR)$^+$ breast cancer from a longitudinal cohort and the autoantibody repertoire of a mouse model engineered to develop ER$^+$ breast cancer (12). We provided evidence for the occurrence of circulating autoantibodies directed against glycolytic pathway proteins preceding a diagnosis of ER$^+$/PR$^+$ breast cancer in samples collected up to 6 months before diagnosis (1). However, there is a paucity of data about the humoral immuneresponse in triple-negative breast cancer (TNBC) and the extent of similarities and differences in the antigenic repertoire between TNBC and ER$^+$ breast cancer. TNBC represents an aggressive type with poor prognosis and has been associated with distinct gene expression signatures with a predominance of a basal expression subtype (13). The basal subtype correlates with high histologic grade at the time of diagnosis (14).

In the present study, we addressed the occurrence of autoantibodies associated with TNBC. High-density protein arrays prepared from lysate proteins from the MDA-MB-231 cell line were probed with plasma samples collected before clinical diagnosis of TNBC from participants in the Women's Health Initiative (WHI)

[1]MD Anderson Cancer Center, Houston, Texas. [2]Fred Hutchinson Cancer Research Center, Seattle, Washington. [3]Tumor Vaccine Group, University of Washington, Seattle, Washington. [4]Division of Preventive Medicine, Brigham & Women's Hospital, Harvard Medical School, Boston, Massachusetts. [5]Division of Hematology/Oncology, Laura and Isaac Perlmutter Cancer Center, New York University Langone Medical Center, New York, New York.

Corresponding Author: Samir Hanash, MD Anderson Cancer Center, 6767 Bertner Ave, Houston, TX 77030. Phone: 713-745-5242; Fax: 713-563-5746; E-mail: shanash@mdanderson.org

doi: 10.1158/0008-5472.CAN-15-0248

Published OnlineFirst June 18, 2015; DOI: 10.1158/0008-5472.CAN-15-0248

cohort (15). The goal was to identify antigens that exhibited differential reactivity with circulating immunoglobulins among cases compared with controls. We also constructed in parallel arrays prepared from lysate proteins of an immortalized cell line derived from the C3(1)-T mouse model that were probed with mouse plasma samples collected before palpable tumor from the same mouse model and from tumor-free control mouse plasmas (16). We further examined using mass spectrometry (MS), the occurrence of antigen–antibody complexes using plasma samples collected at the time of diagnosis of early-stage TNBC. The potential occurrence of a distinctive autoantibody repertoire in TNBC was examined through a comparison with our prior findings in ER^+PR^+ breast cancer.

Materials and Methods

Plasma samples

Prediagnostic EDTA plasma samples were collected as part of the WHI observational study (Table 1). Plasma was available from 13 women who subsequently developed TNBC. Plasma from an equal number of controls from the same cohort matched on age, time of blood collection, and hormone therapy use was analyzed in parallel. EDTA plasma samples were collected from newly diagnosed women with stage II TNBC and used for MS analysis of proteins bound to Ig. Separate analyses were performed using plasmas from 9 premenopausal and 9 postmenopausal women diagnosed with TNBC and from an equal number of control women matched for menopausal status and blood collection and storage conditions.

Plasma samples used for autoantibody studies were collected from a C3(1)-T mouse model that has been engineered to develop hormone-independent, invasive tumors in the mammary epithelium (16). Plasma was collected at baseline, at 8 weeks, and before palpable tumor, on average around 120 days from 19 mice.

Array construction

One hundred fifty milligrams of protein derived from MDA-MB-231 and from C3(1)-T cell lysates was each subjected to orthogonal two-dimensional (2D) high-performance liquid chromatography (HPLC) fractionation in an automated system (Shimadzu Corporation; ref. 17). Fractionation was based on anion exchange (SAX/10 column, 7.5 mm ID × 150 mm, Column Technology Inc) using a 40 step-elution, followed by a second-dimension reversed-phase separation (RP/5D column, 4.6 mm ID × 150 mm, Column Technology Inc). Fractions ($n = 2{,}430$) were collected from the 2D separation. The first-dimension anion-exchange chromatography mobile phase **A** was 20 mmol/L Tris, pH 8.5, and mobile phase **B** was 20 mmol/L Tris, 1 mol/L NaCl, pH 8.5. The second-dimension reversed-phase chromatography mobile phase **A** was 95% water, 5% acetonitrile, 0.1% TFA and mobile phase **B** was 90% acetonitrile, 10% water, 0.1% TFA.

Table 1. Human subject characteristics

	WHI samples	
	Case	**Control**
Sample number	13	13
Average age, y	61 (50–69)	61 (50–69)
Stage		
I	0	—
II	8 (61.5%)	—
III	5 (38.5%)	—
IV	0	—
Avg. days to diagnosis	138.5 (6–240)	—

A total of 300 μL from each fraction was lyophilized and resuspended in 30 μL of printing buffer (250 mmol/L Tris-HCl, pH 6.8, 0.5% SDS, 25% glycerol, 0.05% Triton X-100, 62.5 mmol/L dithiothreitol). Fractions ($n = 1{,}950$), together with printing buffer as negative controls and positive controls, were printed onto nitrocellulose-coated slides using a contact printer, as previously described (6, 18). Plasma samples were hybridized with an individual microarray at a dilution of 1:150. Reactivity was quantified using an indirect immunofluorescence protocol. Local background subtracted median spot intensities were generated using GenePix Pro 6.1 and used for downstream statistical analysis using R 2.9.0. Spot intensities were log (base 2) transformed before statistical analysis. *P* values were calculated using the Student *t* test.

Western blots

Individual fractions (100 μL) were lyophilized and resuspended in 40 μL of loading buffer. Fractions were run in separate lanes of a 4% to 12% Bis-Tris Criterion XT Precast Gel. Gels were transferred to polyvinylidene difluoride (PVDF) membranes for 1.5 hours at 80 V. Membranes were blocked in 3% BSA at room temperature for 1 hour. Plasma samples were diluted 1:500 in 3% BSA and incubated with the membrane at 4°C overnight. Samples were removed and membranes were washed with 0.1% PBST 5 times for 5 minutes each. Horseradish peroxidase–labeled anti-mouse or anti-human IgG at a 1:2,000 dilution was incubated with the membrane at room temperature for 1 hour. Solutions were removed and membranes were washed with 0.1% PBST 5 times for 5 minutes each. Membranes were exposed to enhanced chemiluminescence (ECL) for 1 minute and exposed to ECL hyperfilm for varied lengths of time. Films were developed and scanned for qualitative analysis.

Identification of immunogenic proteins in microarray reactive fractions

Immunogenic proteins were identified as previously described (1, 19). Briefly, significantly elevated fractions and neighboring fractions were grouped into "fraction clusters" on the basis of microarray reactivity and subjected to further analysis. Western blot analysis was used to determine the molecular weight of proteins with autoantibody reactivity in plasma samples by matching observed bands to microarray reactivity data. MS analysis matched total peptide count from individual fractions to microarray reactivity data to determine protein identifications. When no reactive bands were observed in Western blot analyses, protein identification was based solely on results from the MS analysis of fractions.

On the basis of the protein microarray analysis, 50 μL of each reactive fraction from the 2D-HPLC was lyophilized using a freeze drying system (Labconco). The lyophilized protein samples were dissolved in 100 mmol/L NH_4HCO_3 (pH 8.5) followed by overnight in-solution digestion with trypsin at 37°C. The digestion was quenched by adding 5 μL of 1.0% formic acid solution before LC-MS/MS analysis as described previously (20). Briefly, peptides were separated by reversed-phase chromatography using a *nano* HPLC system (Eksigent) coupled online with a LTQ-FT mass spectrometer (Thermo Fisher Scientific, Inc.). MS parameters were spray voltage 2.5 kV, capillary temperature 200°C, FT resolution 100,000, FT target value 8×10^5, LTQ target value 10^4, 1 FT

Published OnlineFirst June 18, 2015; DOI: 10.1158/0008-5472.CAN-15-0248

microscan with 850 ms injection time, and 1 LTQ microscan with 100 ms injection time. Mass spectra were acquired in a data-dependent mode with the m/z range of 400 to 2,000. The full mass spectrum (MS scan) was acquired by the FT and tandem mass spectrum (MS/MS scan) was acquired by the LTQ with a 35% normalized collision energy. Acquisition of each full mass spectrum was followed by the acquisition of MS/MS spectra for the 5 most intense +2 or +3 ions within a 1-second duty cycle. The minimum signal threshold (counts) for a precursor occurring during a MS scan was set at 1,000 for triggering a MS/MS scan.

The acquired LC-MS/MS data were processed by the Computational Proteomics Analysis System (9, 21, 22). Briefly, LC-MS/MS data were first converted to mzXML format using ReAdW software (version 1.2) to generate the peak list for protein database searching. The X!Tandem search engine (version 2005.12.01) parameters included cysteine (Cys) alkylated with iodoacetamide (57.02146@C) as a fixed modification and methionine (Met) oxidation (15.99491@M) as a variable modification. Data were searched against the International Protein Index (IPI) human protein knowledgebase (version v3.57), which contained entries for 76,542 proteins. The minimum criterion for peptide matching was a Peptide Prophet Score $\geq$ 0.2. Peptides meeting this criterion were grouped to protein sequences using the Protein Prophet algorithm at an error rate of $\leq$5%. Total peptide count in each fraction was used as a measure of protein concentration within that fraction.

Analysis of Ig-bound proteins in plasma by MS

IgG-bound proteins from a total of 100 μL of plasma for each experimental condition were extracted with Protein A/G Agarose (Thermo Scientific, #20421 20422 20423). The collected proteins were treated with 25 mmol/L TCEP for Cys reduction and subsequently alkylated with acrylamide. The samples were next fractionated at the protein level by reverse-phase chromatography followed by desalting for 5 minutes with 95% mobile phase A (0.1% TFA in 95% H_2O) at a flow rate of 3 mL/min. Proteins were eluted from the column and collected into 12 fractions, at a flow rate of 2.1 mL/min, with a gradient elution that included an increase from 5% to 70% mobile phase B (0.1% TFA in 95% acetonitrile) over 25 minutes, 70% to 95% mobile phase B for 3 minutes, a wash step to hold at 95% mobile phase B for 2 minutes, and a re-equilibration step at 95% mobile phase A for 5 minutes. The collected fractions were lyophilized and digested with trypsin before analysis by MS using a SYNAPT G_2–S instrument and Waters Masslynx (version 4.1, SCN 851). The mass spectrometer was operated in V-mode with a typical resolving power of at least 20,000. All analyses were performed using positive mode ESI using a NanoLockSpray source. The lock mass channel was sampled every 60 seconds. The mass spectrometer was calibrated with a fibrinopeptide solution (300 fmol/μL) delivered through the reference sprayer of the NanoLockSpray source. Accurate mass LC-HDMSE data was collected in an alternating, low-energy (MS) and high-energy (MSE) mode of acquisition with mass scan range from m/z 50 to 1800. The spectral acquisition time in each mode was 1.0 second with a 0.1-second interscan delay. In low-energy HDMS mode, data were collected at constant collision energy of 2 eV in both Trap cell and Transfer cell. In high-energy HDMSE mode, the collision energy was ramped from 25 to 55 eV in the Transfer cell only. The RF applied to the quadrupole mass analyzer was adjusted such that ions from m/z 300 to 2,000 were efficiently transmitted, ensuring that any ions observed in the LC-HDMSE data less than m/z 300 were known to arise from dissociations in the Transfer collision cell. The acquired LC-HDMSE data were processed and searched against protein knowledge database (Uniprot) through ProteinLynx Global Server (PLGS, Waters Company) with false discovery rate (FDR) 4%.

Results

Autoantibody profiles in human TNBC prediagnostic plasmas

Prediagnostic plasmas were available from 13 women who were participants in the postmenopausal WHI cohort study and who were diagnosed with TNBC up to 240 days subsequent to blood collection (Table 1). We also obtained from the same cohort, plasmas from an equal number of matched healthy controls that remained cancer-free during the period of follow-up. The prediagnostic period of 240 days was similar to the 259 days of the prior WHI ER^+ plasma autoantibody study (1). Plasma samples were each individually hybridized with MDA-MB-231–derived protein arrays. Of the 2,300 printed fractions from the MDA-MB-231 human breast cancer cell line, 229 individual fractions had significantly elevated IgG reactivity ($P < 0.01$ and mean ratio >2) in preclinical plasmas compared with control plasmas. Concordant reactivity among some neighboring fractions suggested elution of reactive antigens over sequential chromatographic fractions. These peak reactivity profiles were used to select clusters around statistically significant fractions. MS yielded identification of 49 reactive proteins (Table 2).

Ingenuity network analysis of reactive proteins identified in human samples revealed top network functions that included cancer and cellular morphology. Top scoring networks exhibited major nodes of PI3K and TP53, genes commonly mutated in TNBC (Fig. 1A and B). An enrichment was also observed for cytoskeletal proteins consisting of actins, cytokeratins, DNAH11, LASP1, and ZYX (FDR = 3.8E−9). Reactive cytokeratins consisted of KRT1, 2, 5, 6a, 9, 10, 14, and 16. The cytokeratin signature was not previously observed in ER^+ breast cancer (1). An enrichment was also observed for spliceosome proteins represented by HNRNPK, SF3B1, SFRS1, 2, 3, 7, and 9 (FDR = 7.5E−4) as previously observed in ER^+ breast cancer (1). We also investigated circulating protein complexes of proteins in the glycolytic pathway by Western blotting using WHI TNBC case samples and matched controls, which revealed an increase in circulating immune complexes involving glycolytic proteins, notably PKM2, ENO1, and TPI, in cases compared with controls as we previously observed in ER^+ breast cancer, in samples collected 0 to 33 weeks before diagnosis compared with farther from diagnosis (Fig. 2A; ref. 1).

Autoantibody profiles in plasmas from a TNBC mouse model before occurrence of palpable tumor

Plasma samples collected at baseline and before palpable tumor from 19 individual mice were each hybridized with mouse breast cancer cell lysate protein arrays. Of the 2,800 printed fractions, 148 individual fractions exhibited significantly increased Ig binding ($P < 0.01$ and mean ratio >2) in preclinical samples compared with baseline. Analysis of reactive clusters yielded identification of 33 reactive proteins (Table 3) from the C3(1)-T mouse model. A spliceosome autoantibody signature was observed in plasmas from the C3(1)-T mouse model, as we observed with human prediagnostic TNBC samples and as we previously reported in preclinical plasmas from an ER^+ breast

Published OnlineFirst June 18, 2015; DOI: 10.1158/0008-5472.CAN-15-0248

Table 2. Immunogenic proteins identified by autoantibody responses from patients with TNBC to MDA-MB-231 cancer cell lysate

Gene	Description	Subcellular localization	Case-to-control ratio	*q*	AUC
ACTA1	Actin, alpha 1, skeletal muscle	Cytoplasm	2.17	1.59E−03	0.825
ACTA2	Actin, alpha 2, smooth muscle, aorta	Cytoplasm	2.17	1.59E−03	0.825
ACTB	Actin, beta	Cytoplasm	2.34	4.30E−05	0.959
ACTC1	Actin, alpha, cardiac muscle 1	Cytoplasm	2.34	4.30E−05	0.959
ACTG1	Actin, gamma 1	Cytoplasm	2.17	1.59E−03	0.825
ACTG2	Actin, gamma 2, smooth muscle, enteric	Cytoplasm	2.17	1.59E−03	0.825
AHNAK	AHNAK nucleoprotein	Nucleus	2.50	4.73E−03	0.846
BAD	BCL2-associated agonist of cell death	Cytoplasm	2.55	2.06E−05	0.923
CALU	Calumenin	Cytoplasm	2.13	4.58E−03	0.811
CLTA	Clathrin, light chain A	Plasma Membrane	2.41	4.46E−03	0.861
CLTB	Clathrin, light chain B	Plasma Membrane	2.29	8.71E−05	0.899
DCD	Dermcidin	Extracellular Space	2.00	2.32E−03	0.837
DNAH11	Dynein, axonemal, heavy chain 11	Cytoplasm	2.41	4.46E−03	0.861
EIF4B	Eukaryotic translation initiation factor 4B	Cytoplasm	2.71	1.62E−04	0.923
HIST1H1C	Histone cluster 1, H1c	Nucleus	2.34	4.30E−05	0.959
HIST1H1D	Histone cluster 1, H1d	Nucleus	2.14	2.18E−03	0.855
HIST1H1E	Histone cluster 1, H1e	Nucleus	2.07	2.80E−04	0.876
HIST1H1T	Histone cluster 1, H1t	Nucleus	2.79	1.17E−03	0.852
HNRNPK	Heterogeneous nuclear ribonucleoprotein K	Nucleus	2.06	2.54E−03	0.834
HSPA5	Heat shock 70-kDa protein 5	Cytoplasm	2.49	8.01E−03	0.802
KRT1	Keratin 1	Cytoplasm	2.08	1.17E−03	0.828
KRT10	Keratin 10	Cytoplasm	2.10	7.97E−03	0.858
KRT14	Keratin 14	Cytoplasm	2.04	1.42E−03	0.899
KRT16	Keratin 16	Cytoplasm	2.77	2.09E−03	0.899
KRT2	Keratin 2	Cytoplasm	2.28	4.96E−03	0.817
KRT5	Keratin 5	Cytoplasm	2.04	1.42E−03	0.899
KRT6A	Keratin 6A	Plasma membrane	2.77	2.09E−03	0.899
KRT9	Keratin 9	Cytoplasm	2.07	5.13E−04	0.882
LASP1	LIM and SH3 protein 1	Cytoplasm	2.38	1.92E−03	0.879
MRPS36	Mitochondrial ribosomal protein S36	Cytoplasm	2.37	6.47E−03	0.817
NUCB1	Nucleobindin 1	Cytoplasm	2.37	2.01E−03	0.828
P4HB	Prolyl 4-hydroxylase, beta polypeptide	Cytoplasm	2.55	2.06E−05	0.923
PDIA3	Protein disulfide isomerase family A, member 3	Cytoplasm	2.06	2.54E−03	0.834
PRKCSH	Protein kinase C substrate 80K-H	Cytoplasm	2.02	2.28E−03	0.831
RCN1	Reticulocalbin 1, EF-hand calcium-binding domain	Cytoplasm	2.17	8.84E−05	0.923
RPLP2	Ribosomal protein, large, P2	Cytoplasm	2.36	1.02E−04	0.932
RPS21	Ribosomal protein S21	Cytoplasm	2.29	8.71E−05	0.899
RPS27A	Ribosomal protein S27a	Cytoplasm	2.13	3.81E−04	0.911
SF3B1	Splicing factor 3b, subunit 1, 155 kDa	Nucleus	2.33	2.02E−04	0.893
SLIRP	SRA stem-loop interacting RNA-binding protein	Cytoplasm	2.37	7.66E−03	0.811
SFRS1	Serine/arginine-rich splicing factor 1	Nucleus	2.23	2.02E−04	0.914
SFRS2	Serine/arginine-rich splicing factor 2	Nucleus	2.00	6.69E−04	0.882
SFRS3	Serine/arginine-rich splicing factor 3	Nucleus	2.79	1.17E−03	0.852
SFRS7	Serine/arginine-rich splicing factor 7	Nucleus	2.36	1.02E−04	0.932
SFRS9	Serine/arginine-rich splicing factor 9	Nucleus	2.79	1.17E−03	0.852
UBA52	Ubiquitin A-52 residue ribosomal protein fusion product 1	Cytoplasm	2.13	3.81E−04	0.911
UBB	Ubiquitin B	Cytoplasm	2.53	6.71E−03	0.846
UBC	Ubiquitin C	Cytoplasm	2.53	6.71E−03	0.846
ZYX	Zyxin	Plasma membrane	2.06	2.54E−03	0.834

cancer mouse model and ER^+ breast cancer subjects. The spliceosome signature consisted of Hnrnpk, Hnrnpm, Sfrs2, and U2af2. The glycolysis signature previously reported in ER^+ breast cancer was similarly observed in the C3(1)-T mouse preclinical samples, with 3 proteins (Eno1, Pkm2, and Tpi1) associated with glycolysis exhibiting autoantibody reactivity.

Identified Ingenuity Network Analysis of antigenic proteins from the C3(1)-T mouse was done as with human TNBC antigenic proteins. The top two scoring networks ($P \sim 10^{-30}$ and $P \sim 10^{-10}$) included major nodes commonly associated with an invasive, triple-negative, or basal phenotype of breast cancer, encompassing TP53, MDM2, BRCA1, and CDKN1A and cytokeratins (Fig. 3A and B). Gene ontology analysis of proteins associated with autoantibodies (23) yielded a signature of cytoskeletal proteins (FDR = 0.0056), consisting mainly of cytokeratins and vimentin. This signature that included KRT4 6a, 7, 9, 14, 18, and 19 was not previously observed in ER^+ breast cancer mouse or human samples but was concordant with the cytokeratin autoantibody signature observed in prediagnostic TNBC plasmas.

Ig-bound proteins in plasmas from subjects with newly diagnosed TNBC

The occurrence of immune complexes associated with TNBC was further investigated using a MS approach applied to plasmas from subjects with newly diagnosed TNBC and healthy controls matched for menopausal status. The approach was based on capture of the Ig fraction from plasmas followed by MS to identify Ig-bound proteins. The quantitation was based on the MS counts

Published OnlineFirst June 18, 2015; DOI: 10.1158/0008-5472.CAN-15-0248

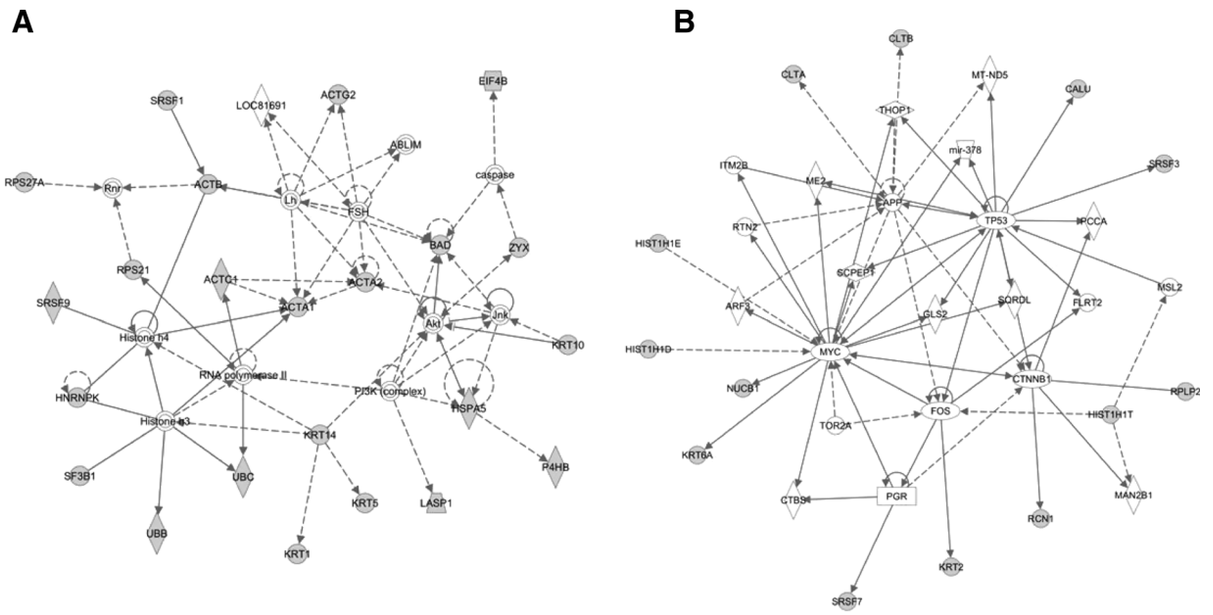

Figure 1.
A and B, top two networks of proteins eliciting a significantly elevated ($P < 0.01$; mean ratio > 2) autoimmune response in WHI human prediagnostic TNBC samples, based on Ingenuity Pathway Analysis.

calculated from the cumulative number of the MS2 spectra assigned to each protein accession. To this effect, 9 plasma samples from premenopausal women and 9 samples from postmenopausal newly diagnosed women with stage II TNBC and an equal number of plasmas from healthy pre- and postmenopausal women were separately pooled, and individual pools were subjected to MS analyses of Ig-bound fractions. We identified and quantified a total of 90 and 45 Ig-bound proteins from

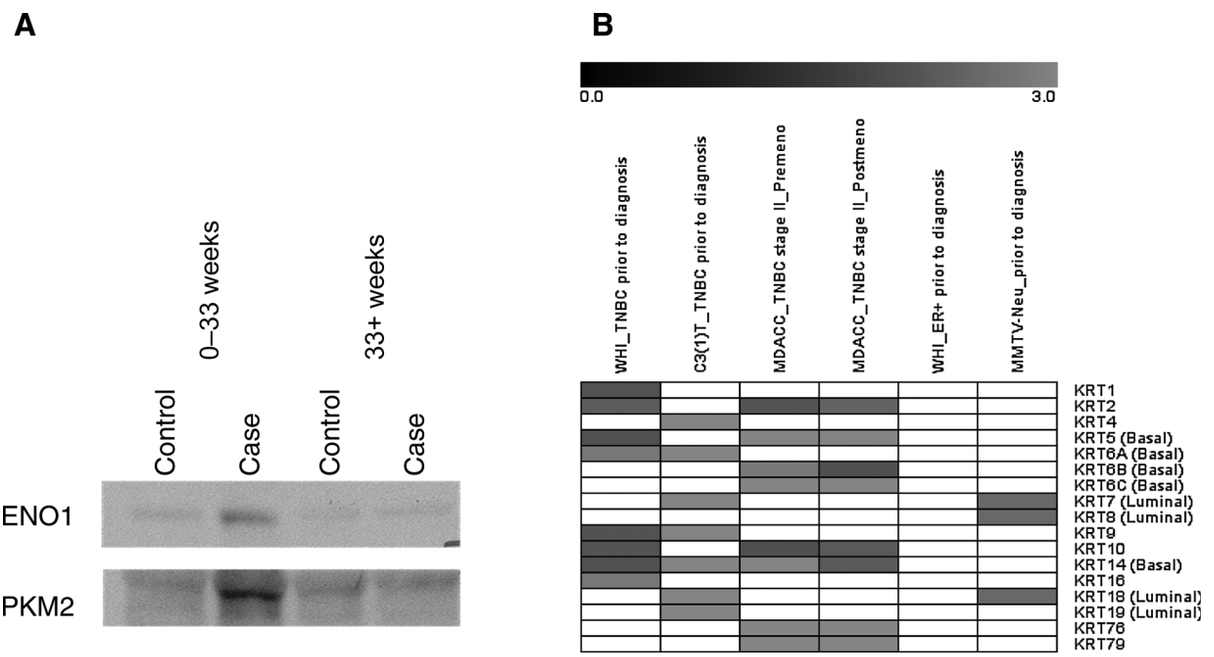

Figure 2.
Signatures of autoimmune response in plasma. A, Western blot analysis of immunodepleted fractions from pooled prediagnostic TNBC samples collected within 33 weeks before diagnosis and greater than 33 weeks before diagnosis compared with matched controls for glycolysis pathway proteins ENO1 and PKM2. Increased reactivity is observed in samples collected within 33 weeks before diagnosis. B, cytokeratin autoantibody panel in TNBC/basal and ER^+/luminal type. Gray indicates statistically significant and elevated in case. WHI ER^+ and MMTV-Neu dataset was from our previous study (1).

Published OnlineFirst June 18, 2015; DOI: 10.1158/0008-5472.CAN-15-0248

Table 3. Immunogenic proteins identified in C3(1)-T mouse cancer cell lysate

Gene	Description	Subcellular localization	Case-to-control ratios	q[a] Time point #1	q[a] Time point #2
Adamts2	ADAM metallopeptidase with thrombospondin type 1 motif, 2	Extracellular space	4.98	2.52E−03	2.38E−03
Dkc1	Dyskeratosis congenita 1, dyskerin	Nucleus	4.98	2.52E−03	2.38E−03
Eif5a	Eukaryotic translation initiation factor 5A	Cytoplasm	4.48	2.49E−03	7.04E−03
Eno1	Enolase 1, (alpha)	Cytoplasm	6.23	7.39E−04	1.89E−03
Hnrnpk	Heterogeneous nuclear ribonucleoprotein k	Nucleus	4.08	1.49E−03	6.70E−04
Hnrnpm	Heterogeneous nuclear ribonucleoprotein m	Nucleus	4.74	1.50E−03	4.36E−03
Hspa5	Heat shock 70-kDa protein 5 (glucose-regulated protein, 78 kDa)	Cytoplasm	4.95	2.49E−03	6.14E−03
Hspa9	Heat shock 70-kDa protein 9 (mortalin)	Cytoplasm	4.15	6.64E−03	2.69E−03
Idh3a	Isocitrate dehydrogenase 3 (NAD+) alpha	Cytoplasm	3.86	6.31E−05	5.75E−05
Krt14	Keratin 14	Cytoplasm	8.80	1.09E−03	9.39E−03
Krt18	Keratin 18	Cytoplasm	4.46	1.23E−04	4.51E−03
Krt19	Keratin 19	Cytoplasm	3.69	1.22E−04	8.42E−05
Krt4	Keratin 4	Cytoplasm	6.91	2.97E−03	2.89E−03
Krt6a	Keratin 6A	Plasma membrane	4.74	1.50E−03	4.36E−03
Krt7	Keratin 7	Cytoplasm	4.10	1.52E−03	1.39E−03
Krt9	Keratin 9	Cytoplasm	3.69	1.22E−04	8.42E−05
Nup153	Nucleoporin 153 kDa	Nucleus	6.91	2.97E−03	2.89E−03
Ogfr	Opioid growth factor receptor	Plasma membrane	4.98	2.52E−03	2.38E−03
Pdia3	Protein disulfide isomerase family A, member 3	Cytoplasm	5.12	1.97E−03	2.43E−03
Pdia6	Protein disulfide isomerase family A, member 6	Cytoplasm	4.31	1.33E−03	5.46E−04
Pkm2	Pyruvate kinase, muscle	Cytoplasm	5.12	1.97E−03	2.43E−03
Psmc3	Proteasome (prosome, macropain) 26S subunit, ATPase, 3	Nucleus	3.86	6.31E−05	5.75E−05
Ptbp1	Polypyrimidine tract-binding protein 1	Nucleus	4.11	3.03E−04	2.40E−03
S100a11	S100 calcium-binding protein A11	Cytoplasm	5.54	3.15E−03	4.78E−03
Sfrs12	Serine/arginine-rich splicing factor 12	Nucleus	3.86	6.31E−05	5.75E−05
Sfrs2	Serine/arginine-rich splicing factor 2	Nucleus	3.87	2.22E−03	3.12E−03
Stxbp3a	Syntaxin-binding protein 3	Plasma membrane	4.87	2.17E−03	1.90E−03
Tpi1	Triosephosphate isomerase 1	Cytoplasm	4.70	5.50E−03	7.21E−03
U2af2	U2 small-nuclear ribonucleoprotein auxiliary factor (U2AF) 2	Nucleus	3.86	6.31E−05	5.75E−05
Ubb	Ubiquitin B	Cytoplasm	3.87	2.22E−03	3.12E−03
Ubc	Ubiquitin C	Cytoplasm	3.87	2.22E−03	3.12E−03
Vim	Vimentin	Cytoplasm	5.89	4.27E−04	5.10E−05
Whsc1	Probable histone-lysine *N*-methyltransferase NSD2	Nucleus	4.48	2.49E−03	7.04E−03

NOTE: Case-to-control ratios are an average of two analyzed blood draws.
[a]q values based on all 2,808 arrayed fractions.

premenopausal stage II TNBC case plasmas versus healthy, respectively, and 133 and 123 distinct proteins from postmenopausal stage II TNBC cases plasmas versus healthy, respectively. Of these proteins, 10 met the criteria of 2-fold increase in MS counts in case versus control, as a measure of the amount of protein bound to IG (24) in both the premenopausal and postmenopausal samples (Table 4). These 10 proteins were identified with two or more peptides each. Remarkably, 9 of the 10 common proteins consisted of cytokeratins, including four basal type of cytokeratins (KRT5, 6B, 6C, and 14). Four additional cytokeratins (KRT 15, 16, 17, and 19) met these criteria only in postmenopausal cases.

Discussion

We have investigated the immune response in the form of autoantibodies in TNBC and have compared findings with a previously published study of ER^+ breast cancer that used a similar approach as in this study (1). TNBC is a more aggressive, invasive cancer than receptor-positive breast cancers (25). Concordant findings were observed with human TNBC cancer plasmas and plasmas from the TNBC mouse model. The proteins that exhibited immunoreactivity both in prediagnostic and mouse model plasmas represented two major groupings. One grouping consisted of spliceosome and glycolysis proteins, which was the major grouping of reactive proteins previously observed in ER^+ breast cancer. However, the top scoring networks in prediagnostic TNBC samples exhibited major nodes of TP53 and PI3K, genes commonly mutated in TNBC.

The finding of autoantibodies to antigens related to TP53 and PI3K networks reflects disease pathogenesis in TNBC. Tumors with germline mutations in BRCA1 are more often hormone receptor–negative and are more likely to overexpress TP53 protein (26–28). TNBC shares clinical and pathologic features with hereditary BRCA1-related breast cancers (29). MDM2 is an important negative regulator of TP53 and has been shown to be integral to metastasis and tumor growth (30). Moreover studies have shown that inhibition of MDM2 reduced systemic inflammation and reduced autoantibody production (31). A network involving PI3K also included CDKN1A and IL5 as additional nodes. The PI3K pathway has been investigated as a therapeutic target for TNBC and basal-type cancers (32, 33). Genetic variants of CDKN1A have been associated with breast cancer and TNBC cell proliferation (34). IL5 plays an important role in immune response by stimulating B cells and increasing immunoglobulin secretion (35) and has been shown to promote malignant pleural effusion formation, which in breast cancer is associated with poor prognosis and reduced survival (36). It is therefore likely that altered pathways in TNBC impact the immune response in the form of autoantibodies.

Published OnlineFirst June 18, 2015; DOI: 10.1158/0008-5472.CAN-15-0248

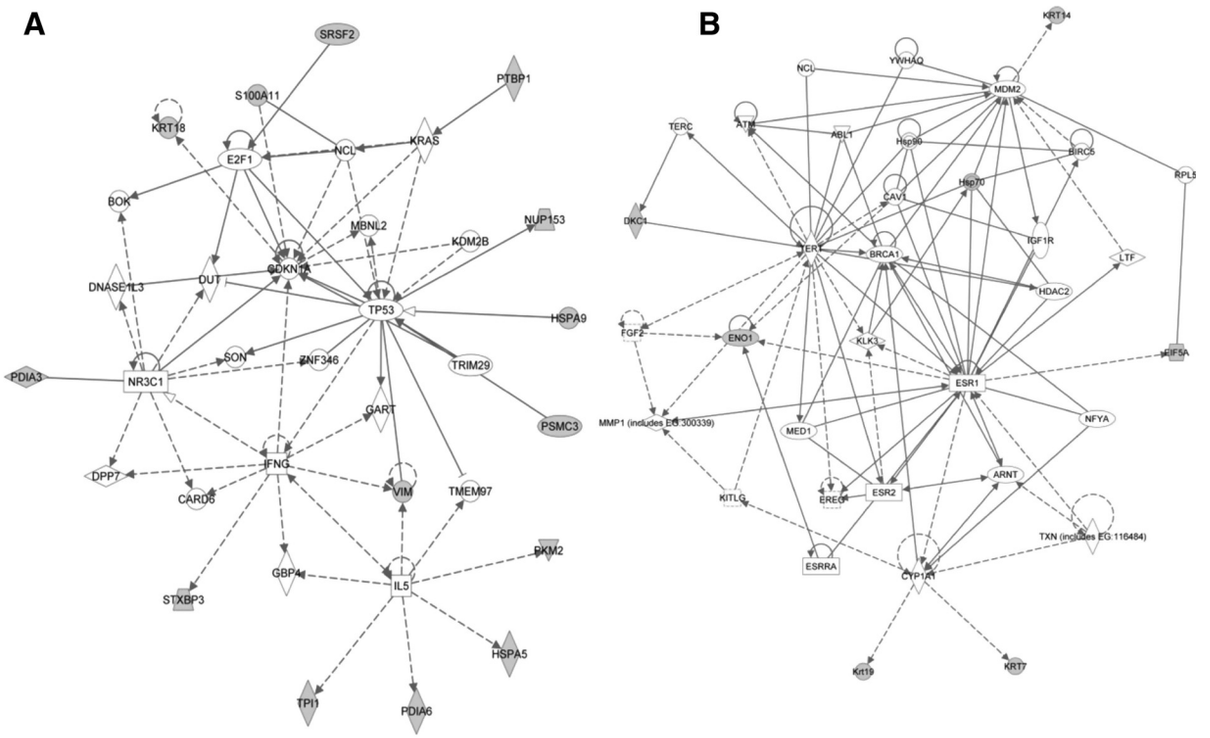

Figure 3.
A and B, top two networks of proteins eliciting a significantly elevated ($P < 0.01$; mean ratio > 2) response in C3(1)-T TNBC mouse model samples collected before palpable tumor compared with baseline, based on Ingenuity Pathway Analysis.

One feature that differentiates TNBC from ER^+ breast cancer is the frequent occurrence of epithelial-to-mesenchymal transition (EMT), a mechanism whereby epithelial cells gain invasive traits. EMT has been correlated with high histologic grade, triple-negative phenotype, and basal-like phenotype breast cancers (37, 38). Alterations in cytoskeletal protein levels have been linked to increases in cell invasion and have been implicated in EMT (39–41).

It is interesting that many of the immunoreactive proteins we have identified are considered to be intracellular proteins. One possible mechanism for their association with an immune response in the form of autoantibodies may be through their occurrence in exosome (42). A recent proteomic study of breast cancer–derived vesicles revealed a large number of glycolysis pathway proteins present, including ALDOA, ENO1, GAPDH, PGK1, and TPI1 (43). Searching against the database Exocarta (44), we found that 35 of the 49 proteins (71%) identified from analysis of human TNBC samples occur in exosomes. In addition, 22 of the 33 (67%) identified proteins from the C3(1)-T mouse also occur in exosomes. Thus, exosomes may contribute as an important antigen-presenting source.

A major finding from our study is the occurrence of a cytokeratin autoantibody signature in prediagnostic human TNBC plasmas as well as in mouse preclinical samples. Moreover, in samples collected at the time of diagnosis, on the basis of the analysis of stage II TNBC samples, cytokeratins represented the most predominant proteins bound to Ig. The autoantibody response in the mouse model and in the prediagnostic samples was investigated using natural protein arrays whereas in samples from newly diagnosed subjects we relied on MS to identify Ig-bound proteins.

Table 4. Plasma IgG-bound proteins in healthy controls and newly diagnosed TNBC stage II patients

Protein	Healthy premenopausal MS counts	TNBC premenopausal MS counts	Healthy postmenopausal MS counts	TNBC postmenopausal MS counts
KRT2	60	130	100	243
KRT5	5	40	18	110
KRT6B	16	46	34	70
KRT6C	2	28	15	50
KRT10	93	188	139	312
KRT14		10	21	47
KRT25	5	28	15	33
KRT76		12	4	21
KRT79	1	12	5	30
LATS1	3	10	4	12

The concordance of findings in independent sample sets and with the use of two different methodologies provides strong support for a basal cytokeratin autoantibody signature associated with TNBC. Multiple cytokeratin family members may be expressed in a given cell and are characteristic of the cell type and differentiation state. Cytokeratins are used for the fingerprinting of carcinomas in general. In breast tissue, the luminal epithelial cells express cytokeratins 8/18, 7, and 19, whereas basal/myoepithelial cells express cytokeratins 5/6, 14, and 17 predominantly (45). Cytokeratins 8 and 18 have been identified as tumor antigens with elevated serum levels of corresponding autoantibodies in patients with several cancer types (46, 47). Several of the cytokeratins found to be associated with autoantibodies in this study have been associated with TNBC and basal type of breast cancer. In one study, a series of 995 invasive breast cancers were investigated using immunohistochemical staining for four basal cytokeratins (48). Expression was demonstrated for KRT5, 6, 14, and 17. Another study found that in three-dimensional organoid assays, collective invasion was led by specialized cancer cells that were defined by their expression of basal epithelial genes, including cytokeratins 5 and 14 (49). Relocalization of KRT5 and KRT14 to the cell surface "leading edge" may contribute to the development of autoantibodies.

A comparison of cytokeratin autoantibodies we previously observed in ER^+/luminal type of breast cancer with TNBC cytokeratin autoantibodies in this study as displayed in Fig. 2B reveals that luminal cytokeratins KRT7, 8, and 18 were commonly observed. Whereas basal cytokeratins were limited to TNBC mouse and human samples providing support for autoantibody signatures reflecting molecular characteristics of TNBC and disease pathogenesis.

Disclosure of Potential Conflicts of Interest

M.L. Disis reports receiving a commercial research grant from EMD Serono and Ventirx and has an ownership interest in Eptihany, Ventirx, and the University of Washington.

Authors' Contributions

Conception and design: H. Katayama, J.J. Ladd, T. Chao, M.L. Disis, S. Hanash
Development of methodology: H. Katayama, J.J. Ladd, T. Chao, J. Suo, M.L. Disis
Acquisition of data (provided animals, acquired and managed patients, provided facilities, etc.): H. Katayama, J.J. Ladd, M.M. Johnson, T. Chao, M. Capello, J. Suo, J. Mao, J.A.E. Manson, R. Prentice, F. Esteva, H. Wang, M.L. Disis
Analysis and interpretation of data (e.g., statistical analysis, biostatistics, computational analysis): H. Katayama, C. Boldt, J.J. Ladd, T. Chao, M. Capello, J.A.E. Manson, F. Esteva, M.L. Disis
Writing, review, and/or revision of the manuscript: H. Katayama, J.J. Ladd, J.A.E. Manson, R. Prentice, F. Esteva, M.L. Disis
Administrative, technical, or material support (i.e., reporting or organizing data, constructing databases): H. Katayama, M.L. Disis
Study supervision: H. Katayama, M.L. Disis, S. Hanash

Grant Support

This work was supported by an NCI grant U01CA141539 and a Komen Foundation grant. S. Hanash was supported by a Rubenstein Family endowed professorship. M.L. Disis was supported by the Athena Distinguished Professorship of Breast Cancer Research and a Komen Leadership Award.

The costs of publication of this article were defrayed in part by the payment of page charges. This article must therefore be hereby marked *advertisement* in accordance with 18 U.S.C. Section 1734 solely to indicate this fact.

Received January 26, 2015; revised April 20, 2015; accepted May 13, 2015; published OnlineFirst June 18, 2015.

References

1. Ladd JJ, Chao T, Johnson MM, Qiu J, Chin A, Israel R, et al. Autoantibody signatures involving glycolysis and splicesome proteins precede a diagnosis of breast cancer among postmenopausal women. Cancer Res 2013;73:1502–13.
2. Taguchi A, Politi K, Pitteri SJ, Lockwood WW, Faca VM, Kelly-Spratt K, et al. Lung cancer signatures in plasma based on proteome profiling of mouse tumor models. Cancer Cell 2011;20:289–99.
3. Brichory F, Beer D, Le Naour F, Giordano T, Hanash S. Proteomics-based identification of protein gene product 9.5 as a tumor antigen that induces a humoral immune response in lung cancer. Cancer Res 2001;61:7908–12.
4. Brichory FM, Misek DE, Yim AM, Krause MC, Giordano TJ, Beer DG, et al. An immune response manifested by the common occurrence of annexins I and II autoantibodies and high circulating levels of IL-6 in lung cancer. Proc Natl Acad Sci U S A 2001;98:9824–9.
5. Lu H, Goodell V, Disis ML. Humoral immunity directed against tumor-associated antigens as potential biomarkers for the early diagnosis of cancer. J Proteome Res 2008;7:1388–94.
6. Qiu J, Madoz-Gurpide J, Misek DE, Kuick R, Brenner DE, Michailidis G, et al. Development of natural protein microarrays for diagnosing cancer based on an antibody response to tumor antigens. J Proteome Res 2004;3:261–7.
7. Chaput N, Conforti R, Viaud S, Spatz A, Zitvogel L. The Janus face of dendritic cells in cancer. Oncogene 2008;27:5920–31.
8. Whiteside TL. The tumor microenvironment and its role in promoting tumor growth. Oncogene 2008;27:5904–12.
9. Rauch A, Bellew M, Eng J, Fitzgibbon M, Holzman T, Hussey P, et al. Computational Proteomics Analysis System (CPAS): an extensible, open-source analytic system for evaluating and publishing proteomic data and high throughput biological experiments. J Proteome Res 2006;5:112–21.
10. Heo CK, Bahk YY, Cho EW. Tumor-associated autoantibodies as diagnostic and prognostic biomarkers. BMB Rep 2012;45:677–85.
11. Murphy MA, O'Leary JJ, Cahill DJ. Assessment of the humoral immune response to cancer. J Proteomics 2012;75:4573–9.
12. Lu H, Ladd J, Feng Z, Wu M, Goodell V, Pitteri SJ, et al. Evaluation of known oncoantibodies, HER2, p53, and cyclin B1, in prediagnostic breast cancer sera. Cancer Prev Res 2012;5:1036–43.
13. Xu H, Eirew P, Mullaly SC, Aparicio S. The omics of triple-negative breast cancers. Clin Chem 2014;60:122–33.
14. Rody A, Karn T, Liedtke C, Pusztai L, Ruckhaeberle E, Hanker L, et al. A clinically relevant gene signature in triple negative and basal-like breast cancer. Breast Cancer Res 2011;13:R97.
15. Katayama H, Paczesny S, Prentice R, Aragaki A, Faca VM, Pitteri SJ, et al. Application of serum proteomics to the Women's Health Initiative conjugated equine estrogens trial reveals a multitude of effects relevant to clinical findings. Genome Med 2009;1:47.
16. Green JE, Shibata MA, Yoshidome K, Liu ML, Jorcyk C, Anver MR, et al. The C3(1)/SV40 T-antigen transgenic mouse model of mammary cancer: ductal epithelial cell targeting with multistage progression to carcinoma. Oncogene 2000;19:1020–7.
17. Wang H, Hanash S. Multi-dimensional liquid phase based separations in proteomics. J Chromatogr B Analyt Technol Biomed Life Sci 2003;787:11–8.
18. Madoz-Gurpide J, Kuick R, Wang H, Misek DE, Hanash SM. Integral protein microarrays for the identification of lung cancer antigens in sera that induce a humoral immune response. Mol Cell Proteomics 2008;7:268–81.
19. Qiu J, Choi G, Li L, Wang H, Pitteri SJ, Pereira-Faca SR, et al. Occurrence of autoantibodies to annexin I, 14-3-3 theta and LAMR1 in prediagnostic lung cancer sera. J Clin Oncol 2008;26:5060–6.
20. Wang H, Hanash SM. Increased throughput and reduced carryover of mass spectrometry-based proteomics using a high-efficiency nonsplit nanoflow parallel dual-column capillary HPLC system. J Proteome Res 2008;7:2743–55.

Published OnlineFirst June 18, 2015; DOI: 10.1158/0008-5472.CAN-15-0248

21. MacLean B, Eng JK, Beavis RC, McIntosh M. General framework for developing and evaluating database scoring algorithms using the TANDEM search engine. Bioinformatics 2006;22:2830–2.
22. Nesvizhskii AI, Keller A, Kolker E, Aebersold R. A statistical model for identifying proteins by tandem mass spectrometry. Anal Chem 2003;75: 4646–58.
23. Thomas PD, Kejariwal A, Campbell MJ, Mi H, Diemer K, Guo N, et al. PANTHER: a browsable database of gene products organized by biological function, using curated protein family and subfamily classification. Nucleic Acids Res 2003;31:334–41.
24. Nielsen CT, Ostergaard O, Stener L, Iversen LV, Truedsson L, Gullstrand B, et al. Increased IgG on cell-derived plasma microparticles in systemic lupus erythematosus is associated with autoantibodies and complement activation. Arthritis Rheum 2012;64:1227–36.
25. Dent R, Trudeau M, Pritchard KI, Hanna WM, Kahn HK, Sawka CA, et al. Triple-negative breast cancer: clinical features and patterns of recurrence. Clin Cancer Res 2007;13:4429–34.
26. Boyle P. Triple-negative breast cancer: epidemiological considerations and recommendations. Ann Oncol 2012;23 Suppl 6:vi7–12.
27. Levy-Lahad E, Friedman E. Cancer risks among BRCA1 and BRCA2 mutation carriers. Br J Cancer 2007;96:11–5.
28. Lakhani SR, Van De Vijver MJ, Jacquemier J, Anderson TJ, Osin PP, McGuffog L, et al. The pathology of familial breast cancer: predictive value of immunohistochemical markers estrogen receptor, progesterone receptor, HER-2, and p53 in patients with mutations in BRCA1 and BRCA2. J Clin Oncol 2002;20:2310–8.
29. Turner NC, Reis-Filho JS, Russell AM, Springall RJ, Ryder K, Steele D, et al. BRCA1 dysfunction in sporadic basal-like breast cancer. Oncogene 2007; 26:2126–32.
30. Shi W, Meng Z, Chen Z, Hua Y, Gao H, Wang P, et al. RNA interference against MDM2 suppresses tumor growth and metastasis in pancreatic carcinoma SW1990HM cells. Mol Cell Biochem 2014;387:1–8.
31. Allam R, Sayyed SG, Kulkarni OP, Lichtnekert J, Anders HJ. Mdm2 promotes systemic lupus erythematosus and lupus nephritis. J Am Soc Nephrol 2011;22:2016–27.
32. Kimbung S, Biskup E, Johansson I, Aaltonen K, Ottosson-Wadlund A, Gruvberger-Saal S, et al. Co-targeting of the PI3K pathway improves the response of BRCA1 deficient breast cancer cells to PARP1 inhibition. Cancer Lett 2012;319:232–41.
33. Moulder SL. Does the PI3K pathway play a role in basal breast cancer? Clin Breast Cancer 2010;10 Suppl 3:S66–71.
34. De Santi M, Galluzzi L, Lucarini S, Paoletti MF, Fraternale A, Duranti A, et al. The indole-3-carbinol cyclic tetrameric derivative CTet inhibits cell proliferation via overexpression of p21/CDKN1A in both estrogen receptor-positive and triple-negative breast cancer cell lines. Breast Cancer Res 2011;13:R33.
35. Ikutani M, Yanagibashi T, Ogasawara M, Tsuneyama K, Yamamoto S, Hattori Y, et al. Identification of innate IL-5-producing cells and their role in lung eosinophil regulation and antitumor immunity. J Immunol 2012; 188:703–13.
36. dos Santos GT, Prolla JC, Camillo ND, Zavalhia LS, Ranzi AD, Bica CG. Clinical and pathological factors influencing the survival of breast cancer patients with malignant pleural effusion. J Bras Pneumol 2012; 38:487–93.
37. Jeong H, Ryu YJ, An J, Lee Y, Kim A. Epithelial-mesenchymal transition in breast cancer correlates with high histological grade and triple-negative phenotype. Histopathology 2012;60:E87–95.
38. Sarrio D, Rodriguez-Pinilla SM, Hardisson D, Cano A, Moreno-Bueno G, Palacios J. Epithelial-mesenchymal transition in breast cancer relates to the basal-like phenotype. Cancer Res 2008;68:989–97.
39. Friedl P, Alexander S. Cancer invasion and the microenvironment: plasticity and reciprocity. Cell 2011;147:992–1009.
40. Klymkowsky MW, Savagner P. Epithelial-mesenchymal transition: a cancer researcher's conceptual friend and foe. Am J Pathol 2009;174:1588–93.
41. Yilmaz M, Christofori G. EMT, the cytoskeleton, and cancer cell invasion. Cancer Metastasis Rev 2009;28:15–33.
42. Klein-Scory S, Kubler S, Diehl H, Eilert-Micus C, Reinacher-Schick A, Stuhler K, et al. Immunoscreening of the extracellular proteome of colorectal cancer cells. BMC Cancer 2010;10:70.
43. Palazzolo G, Albanese NN, G DIC, Gygax D, Vittorelli ML, Pucci-Minafra I. Proteomic analysis of exosome-like vesicles derived from breast cancer cells. Anticancer Res 2012;32:847–60.
44. Mathivanan S, Simpson RJ. ExoCarta: a compendium of exosomal proteins and RNA. Proteomics 2009;9:4997–5000.
45. Lane EB, Alexander CM. Use of keratin antibodies in tumor diagnosis. Semin Cancer Biol 1990;1:165–79.
46. Ahlemann M, Schmitt B, Stieber P, Gires O, Lang S, Zeidler R. Evaluation of CK8-specific autoantibodies in carcinomas of distinct localisations. Anticancer Res 2006;26:783–9.
47. Le Naour F, Brichory F, Misek DE, Brechot C, Hanash SM, Beretta L. A distinct repertoire of autoantibodies in hepatocellular carcinoma identified by proteomic analysis. Mol Cell Proteomics 2002;1:197–203.
48. Alshareeda AT, Soria D, Garibaldi JM, Rakha E, Nolan C, Ellis IO, et al. Characteristics of basal cytokeratin expression in breast cancer. Breast Cancer Res Treat 2013;139:23–37.
49. Cheung KJ, Gabrielson E, Werb Z, Ewald AJ. Collective invasion in breast cancer requires a conserved basal epithelial program. Cell 2013;155: 1639–51.

Published OnlineFirst June 18, 2015; DOI: 10.1158/0008-5472.CAN-15-0248

Cancer Research
The Journal of Cancer Research (1916–1930) | The American Journal of Cancer (1931–1940)

AACR American Association for Cancer Research

An Autoimmune Response Signature Associated with the Development of Triple-Negative Breast Cancer Reflects Disease Pathogenesis

Hiroyuki Katayama, Clayton Boldt, Jon J. Ladd, et al.

Cancer Res 2015;75:3246-3254. Published OnlineFirst June 18, 2015.